Metals and Materials International (2021) 27:4477–4486
https://doi.org/10.1007/s12540-020-00663-3

Microstructure, Thermal Conductivity and Mechanical Properties of the Mg–Zn–Sb Ternary Alloys

Yujian Huang[1] · Xiong Zhou[1] · Jun Du[1]

Received: 3 January 2020 / Accepted: 20 February 2020 / Published online: 9 March 2020
© The Korean Institute of Metals and Materials 2020

Abstract
A novel Mg alloys of Mg–xZn–ySb (x = 0, 2, 4, 6; y = 0, 0.2, 0.5, 0.8, 1.2) were designed and their microstructure, thermal conductivity and mechanical properties were systematically investigated in the present study. The as-cast Mg–Zn–Sb ternary alloys consist of α-Mg, Mg_4Zn_7 and Mg_3Sb_2 phases. Sb addition can refine the eutectic structure (α-Mg + Mg_4Zn_7) by the growth of Mg_4Zn_7 on Mg_3Sb_2 phases. The thermal conductivity of Mg–Zn–Sb alloys decreased with increasing Sb content. There existed an interactive effect of Zn/Sb on the thermal conductivity of the Mg–Zn–Sb alloys. The negative effect of Sb addition on thermal conductivity of alloys was getting smaller with increasing Zn content in alloys. The negative effect of Mg_3Sb_2 phases on the thermal conductivity of alloys could be weakened by the formation of weak-scattering Mg_4Zn_7 coated on Mg_3Sb_2 phases. The best refinement effect on microstructure could be obtained with 0.8 wt%Sb addition. Mg–4Zn–0.8Sb alloy possess the best comprehensive properties with thermal conductivity of over than 120 W/(m·K) and UTS of 185.6 MPa.

Keywords Mg–Zn–Sb alloys · Thermal conductivity · Second phases · Tensile properties

1 Introduction

In the 5G mobile systems, higher integration density and increased complexity of the circuits lead to increased heat dissipation, and thus an urgent need for effective heat sink materials. As the "21st Century Green Engineering Materials" with high specific strength, excellent electromagnetic shielding, good thermal conductivity and low density, Mg alloys have a great attractiveness for applications of the heat sink in 5G mobile systems [1].

Although pure Mg possesses high thermal conductivity, it is not practical due to the poor mechanical properties; therefore, alloying is necessary in strengthening alloys for wider applications. However, the introduced solute atoms and precipitated second phases will inevitably have a negative effect on the thermal conductivity of alloys. The solute atoms in matrix will disrupt the periodical arrangement of atoms, result in lattice distortion and thus lead to large thermal conductivity decrease. Moreover, the second phases will act as scattering resources for electrons, whose mean free path is regarded as the major determinant of thermal conductivity [2]. It is worth noting that different alloying elements exhibit significant differences in the degree of reducing thermal conductivity. For example, AZ91D alloy, as a representative of commercial Mg alloys, exhibits low thermal conductivity (51 W/(m·K)) due to the large lattice distortion caused by solute aluminium atoms [3, 4]. However, compared to Al and other common alloying elements, Zn, which has the same hcp crystal structure, valency and similar atomic radius with Mg, results in a much smaller decrease in the thermal conductivity of Mg alloys [5]. Compared to Mg–Al and Mg–Gd binary alloys with the same atomic percentage of the solute atoms, the strongest diffraction peak of Mg–Zn shifted slightly. The small deviation in XRD peaks indicated a small lattice distortion caused by solute Zn atoms and hence a small reduction in thermal conductivity [6]. In addition, Pan et al. [7] reported that the specific thermal resistivity of solute elements for Mg alloys was in the following sequence, Zn < Al < Ca < Sn < Mn < Zr. Furthermore, Ying [8] measured the thermal conductivity of Mg–Al, Mg–Zn and Mg–Mn binary alloys and Zn was also regarded as the weakest electron scatter. When the content of Zn was up to 5 wt%, the thermal conductivity of alloy was still as high as 110 W/(m·K)

✉ Jun Du
tandujun@sina.com

[1] Department of Metallic Materials, School of Materials Science and Engineering, South China University of Technology, Wu Shan Road 381, Tianhe District, Guangzhou 510640, People's Republic of China

[5]. Thus, Zn is usually selected as a master element of high thermal conductivity Mg alloys.

However, Mg–Zn alloys exhibit relatively poor mechanical properties, so there is a growing need to find an alloying element that could improve mechanical properties while slightly reducing thermal conductivity. According to the demonstration of Eivani et al. [9], the decrease of thermal conductivity caused by solute element in matrix is about one magnitude order larger than that in second phases. Recently, the result was also confirmed in a quantitative study by Su et al. [10]. Experimental results showed that the reduction in thermal conductivity per at% addition of RE alloying elements in solid solution is about 123.0 W/(m·K), while that of alloying element in second phases is 6.5–16.4 W/(m·K). Therefore, the alloying element with a low solid solubility could effectively contribute to the mechanical properties while slightly reducing thermal conductivity. Hence, Sb, with a negligible solid solubility in Mg matrix and good strengthening effects, is suggested to be a good strengthening element for high thermal conductivity Mg alloys. There have been many researches about the strengthening effects of Sb addition on Mg alloys. Nayyeri et al. [11] studied the effects of Sb addition on the creep resistance of as-cast Mg–5Sn binary alloy. The formation of thermally stable (1228 °C) Mg_3Sb_2 second phases could strengthen both grains and grain boundaries. For common commercial Mg alloys, AZ91 [12], AM50 [13] and AM60 [14], the yield strength and creep resistance at both room temperature and elevated temperature were also improved by Sb addition. For Mg–Zn alloys, Alizadeh et al. [15] proposed that Sb had a great effect on improving both room-temperature and high-temperature mechanical properties of Mg–4Zn alloys by refining the microstructure and the formation of thermally stable Mg_3Sb_2 particles. Besides, the hardness and strength were considerably increased by Sb addition in both as-cast and annealed conditions [16]. However, The effect of Sb addition on the thermal conductivity of Mg–Zn-based alloys has not been studied before.

In the present study, the microstructure, thermal conductivity and mechanical properties of the Mg–xZn–ySb (x = 0, 2, 4, 6; y = 0, 0.2, 0.5, 0.8, 1.2) alloys were systematically investigated. Based on the results, the thermal conductivity is further predicated by modified Maxwell model and Smith-Palmer equation. Finally, the interactive effect of Zn/Sb was discussed, providing a potential method for keeping the balance between thermal conductivity and mechanical properties in alloys.

2 Experimental Procedures

2.1 Sample Preparation

The alloys with nominal compositions (in wt pct) of Mg–xZn–ySb (x = 0, 2, 4, 6; y = 0, 0.2, 0.5, 0.8, 1.2) were prepared by gravity casting. Commercial pure Mg (99.95 wt pct), pure Zn and pure Sb were melted in an electric resistance furnace under the protection of the mixed gas of 99.5 vol% N_2 and 0.5 vol% SF_6. When the commercial pure Mg was melt at 750 °C, pure Zn and pure Sb were added into the melt. The melt was stirred manually for 1 min to ensure a homogeneous composition. For the settlement of impurities, the melt was held for another 10 min, and then it was stirred and poured into a preheated (200 °C) mold to prepare 5 mm thick samples. Mg–Zn and Mg–Sb binary alloys were aging treated at 200 °C for 72 h followed by air cooling to precipitate solute atoms. In order to dissolve Zn or Sb into the Mg matrix as much as possible without overheating, Mg–Zn alloys and Mg–Sb alloys were solution treated at 320 °C and 500 °C for 12 h followed by water quenching immediately.

2.2 Thermal and Electrical Conductivity

The electrical conductivity (σ) at room temperature (298 K) was measured using eddy current conductivity meter (FIRST FD101).

The measured thermal conductivity value was calculated by using Eq. 1 [17]:

$$\lambda = \alpha \times \rho \times c_p \tag{1}$$

where λ is thermal conductivity (W/(m·K)), α is thermal diffusivity (mm^2/s), c_p is specific heat, (J/(g·K)), and ρ is density (g/cm^3). Density (ρ) of the sample was measured by using density balancer (XHB-3000Z II) according to the Archimedes drainage method. The surfaces of thermal diffusivity disk samples (12.7 mm diameter and 3 mm thickness) were painted by carbon-coating before measurement to reduce the reflection of the light pulse. For each alloy with different composition, at least three samples were tested using laser flash method (Netzsch LFA447) at 25 °C. The specific heat capacity was calculated according to the Neumann–Kopp rule using a Netzsch DSC with sapphire as the reference material. The results of thermal diffusivity (α), specific heat (c_p), density (ρ), thermal conductivity (λ) and electrical conductivity (σ) of as-cast Mg–Zn–Sb ternary alloys were listed in Table 1.

2.3 Microstructure Analysis

Samples for microstructural analysis were mechanically grounded, polished and etched by 5% ethanol nitrate solution. The microstructures of the samples were observed using scanning electron microscopy (SEM, ZEISS Merlin) equipped with an energy dispersive X-Max^{N}20 dual detector system (EDS). The content of solute atoms was obtained by averaging at least 10 EDS results randomly pointed in the Mg matrix. Based on SEM images, the volume fractions of

Table 1 Specific heat (c_p), thermal diffusion (α), density (ρ), thermal conductivity (λ) and electrical conductivity (σ) of as-cast Mg–xZn–ySb (x = 0, 2, 4, 6; y = 0, 0.2, 0.5, 0.8, 1.2) alloys

Alloys	c_p (J/(g·K))	α (mm^2/s)	ρ (g/cm^3)	λ (W/(m·K))	σ (MS/m)
Mg	1.030	88.19	1.734	157.51	21.66
Mg–0.2Sb	0.970	90.05	1.733	151.38	20.82
Mg–0.5Sb	1.010	82.14	1.736	144.02	19.81
Mg–0.8Sb	0.967	82.72	1.738	139.02	19.12
Mg–1.2Sb	0.973	79.40	1.742	134.58	18.51
Mg–2Zn	1.033	77.55	1.753	140.43	19.50
Mg–2Zn–0.2Sb	1.019	76.23	1.76	136.71	18.80
Mg–2Zn–0.5Sb	0.996	74.61	1.767	131.31	18.06
Mg–2Zn–0.8Sb	0.980	73.94	1.766	127.97	17.60
Mg–2Zn–1.2Sb	1.002	70.11	1.769	124.28	17.09
Mg–4Zn	0.988	76.06	1.776	133.46	18.35
Mg–4Zn–0.2Sb	0.946	75.34	1.783	127.08	17.48
Mg–4Zn–0.5Sb	1.025	68.34	1.792	125.52	17.26
Mg–4Zn–0.8Sb	0.988	69.41	1.796	123.16	16.94
Mg–4Zn–1.2Sb	0.935	71.49	1.804	120.59	16.59
Mg–6Zn	1.012	66.40	1.816	122.02	16.78
Mg–6Zn–0.2Sb	1.001	66.63	1.813	120.91	16.63
Mg–6Zn–0.5Sb	0.985	66.96	1.819	119.97	16.50
Mg–6Zn–0.8Sb	0.990	66.30	1.817	119.26	16.40
Mg–6Zn–1.2Sb	1.002	65.11	1.825	119.06	16.37

second phases in the as-cast alloys were obtained from the statistics of MATLAB software. X-ray diffraction (XRD) analysis was also conducted using a diffractometer (Dutch PANalytical X'pert^3) with Cu Kα radiation to identify the second phases. To investigate the distribution of second phases with different compositions, the etched as-cast samples were subsequently observed by electron probe microanalyzer (EPMA-1600) equipped with EDAX Genesis.

2.4 Tensile Properties

Tensile samples with a gauge length of 25 mm were taken from as-cast alloys and tested using the computerized testing machine (Shimadzu/AG-X, Japan) at room temperature. According to ASTM E8M-04 standard (sub-size sample, as presented in Fig. 1), the yield strength (YS), ultimate tensile strength (UTS) and ductility were obtained at a strain rate of 1 mm/min.

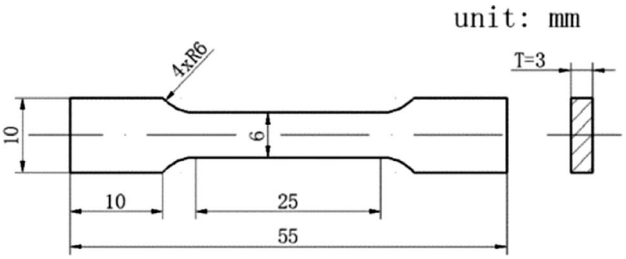

Fig. 1 The dimensions of the tensile specimen

3 Results

3.1 XRD Results

The XRD results (Fig. 2) indicated that as-cast Mg–Zn alloys consisted of α-Mg and Mg_4Zn_7 phases, while as-cast Mg–Zn–Sb alloys consisted of α-Mg, Mg_4Zn_7 and Mg_3Sb_2 phases.

3.2 SEM Microstructure

Figures 3, 4 and 5 show the SEM images of the as-cast Mg–Zn, Mg–Sb and Mg–Zn–Sb alloys, respectively. For Mg–Zn binary alloys (Fig. 3), there was a small amount of Mg_4Zn_7 phases that mainly exhibited a spherical shape and random distribution when the Zn content was less than 4.0 wt%. With increasing Zn content, the second phases became coarser but not developed into continuous networks of eutectic structures.

For Mg–Sb binary alloys, Mg_3Sb_2 phases were sparsely distributed with a spherical shape when Sb content was less than 0.5 wt% (Fig. 4a). The size and volume fraction of Mg_3Sb_2 phases increased with increasing Sb content. Then, semicontinuous networks of rod-like Mg_3Sb_2 phases (Fig. 4c) started to develop in the alloys with Sb content more than 0.8 wt%.

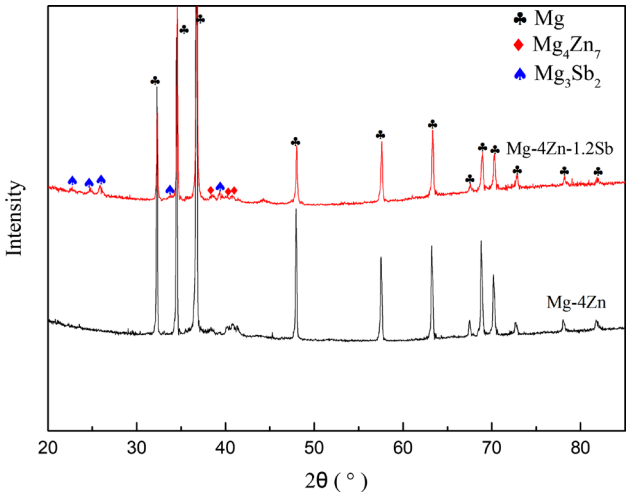

Fig. 2 XRD patterns of Mg–4Zn and Mg–4Zn–1.2Sb alloys

According to the XRD results (Fig. 2) and EDS data (Table 2), Mg–Zn–Sb ternary alloys consist of α-Mg, Mg_3Sb_2 and Mg_4Zn_7 phases. For Mg–2Zn–xSb alloys (Fig. 5a–c), the microstructure consisted mainly of Mg_3Sb_2 phases and only a small amount of Mg_4Zn_7 phases. Therefore, the evolution of second phases with the increase of Sb content was similar to that in Mg–Sb binary alloys. The size and volume fraction of Mg_3Sb_2 phases increased with increasing Sb content. However, semicontinuous networks of rod-like Mg_3Sb_2 phases started to develop in the alloys when Sb content is 1.2 wt% but not 0.8 wt% in Mg–Sb binary alloys. For Mg–6Zn–xSb alloys (Fig. 5d–f), the coarse eutectic structure (α-Mg + Mg_4Zn_7) in Mg–6Zn alloy (Fig. 3c) were significantly refined by Sb addition. At first, the refinement effect increased with increasing Sb content. The best refinement effect can be achieved by adding 0.8 wt% Sb. Then the refinement effect decreased with further increase of Sb content.

3.3 Thermal Conductivity

Figure 6 shows the variation of thermal conductivity of Mg–Zn and Mg–Sb binary alloys with different composition in different heat treatments. With increasing Zn or Sb content, the thermal conductivity of as-cast binary alloys dropped from 157.51 W/(m·K) in commercial pure Mg to 122.51 W/(m·K) in Mg–5Zn alloy, 120.47 W/(m·K) in Mg–2Sb alloy, respectively. Although there were nearly no solute Sb atoms in matrix due to the negligible solid solubility, the thermal conductivity of Mg–Sb alloys was still lower than that of Mg–Zn alloy with the same alloying content. For as-cast Mg–Zn alloys, aging treatment would increase the thermal conductivity of alloys, while solution treatment would decrease it. However, the thermal conductivity of as-cast Mg–Sb alloys changed little after aging or solution treatment.

Table 1 shows the thermal conductivity of as-cast Mg–Zn–Sb alloys with different composition. The thermal conductivity of ternary alloys decreased with increasing Zn and Sb content. Interestingly, the negative effect of Sb addition on the thermal conductivity of alloys is getting smaller with increasing Zn content. For example, the thermal conductivity of Mg–2Zn–1.2Sb alloys was reduced by 11.50% compared with Mg–2Zn alloy; however, the thermal conductivity of Mg–6Zn–1.2Sb alloy was reduced by 2.43% compared with Mg–6Zn alloy.

3.4 Tensile Properties of as-Cast Mg–Zn and Mg–Zn–Sb Alloys

The ultimate strength (UTS), yield strength (YS), and percentage elongation (% EL) values of these alloys are provided in Fig. 7. The Sb addition can effectively improve the ultimate tensile strength (Fig. 7a) and yield strength (Fig. 7b) of Mg–Zn alloys with different Zn content. For example, compared with Mg–4Zn alloy, the ultimate tensile strength

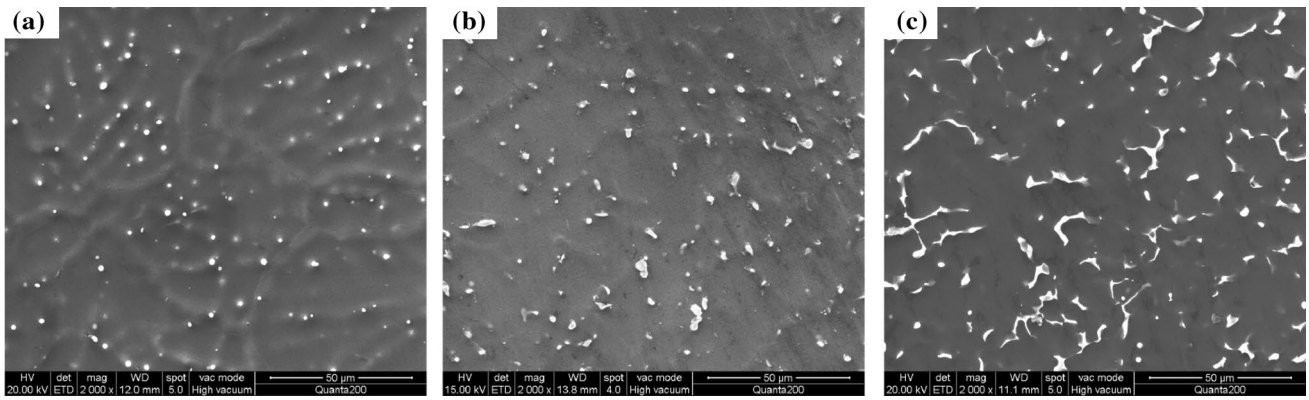

Fig. 3 SEM images of as-cast **a** Mg–2Zn, **b** Mg–4Zn, **c** Mg–6Zn alloys

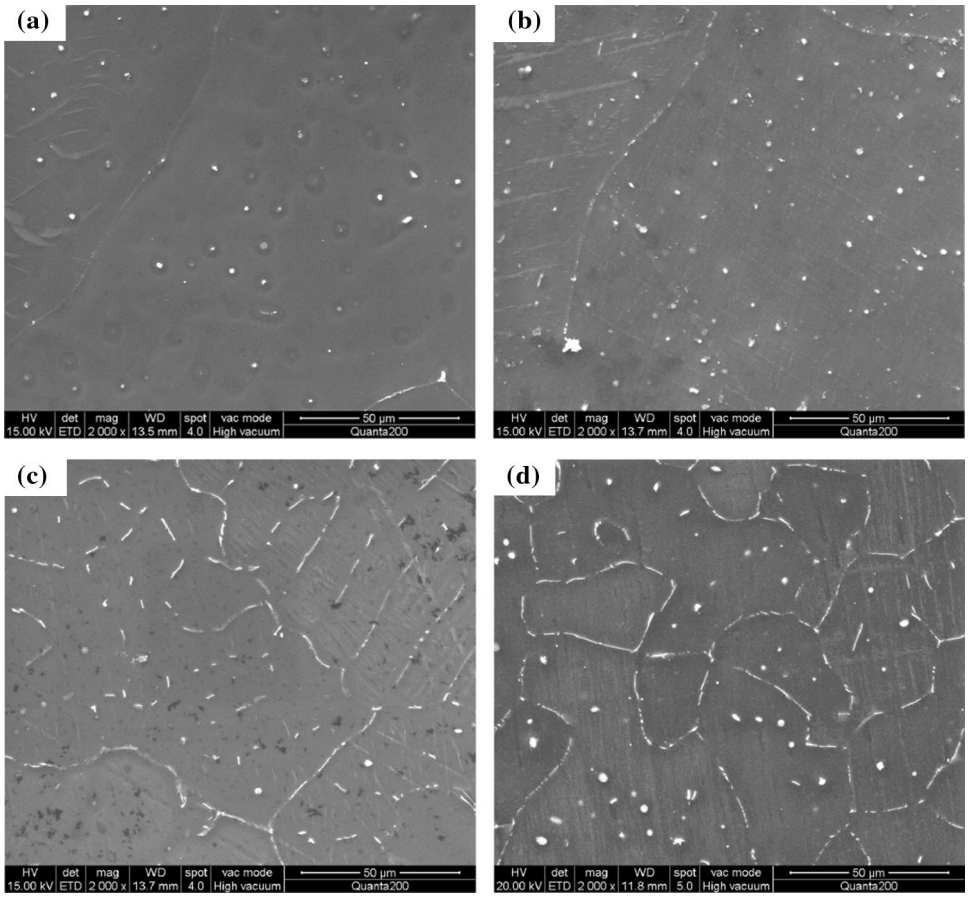

Fig. 4 SEM images of as-cast **a** Mg–0.2Sb, **b** Mg–0.5Sb, **c** Mg–0.8Sb, **d** Mg–1.2Sb alloys

and yield strength of Mg–4Zn–0.8Sb alloy is 185.6 MPa and 62.5 MPa, which is improved by 25.2% and 23.3%, respectively. Figure 7c shows that the EL value of Zn-containing alloys decrease after adding Sb. The Mg–4Zn–0.8Sb alloy possess the best comprehensive tensile properties, UTS of 185.6 MPa, YS of 62.5 MPa and elongation of 19.8% .

4 Discussion

4.1 Microstructure

The difference in the electronegativity values among Mg of 1.31, Zn of 1.6 and Sb of 2.05, suggests that the Sb is tending to form a compound with Mg rather than Zn [16, 18]. Based on the XRD results (Fig. 2) and negligible solid solubility of Sb in Mg matrix, nearly all of the Sb added into Mg–Zn alloys would react with Mg to form Mg_3Sb_2 phases but not Mg–Zn–Sb or Zn–Sb phases, which is consistent with the previous researches [15, 16]. According to the SEM images in Fig. 4, Mg_3Sb_2 phases were mainly distributed in grain-boundaries. Due to the high formation temperature (1245 °C) of Mg_3Sb_2 and the high affinity of Sb to Mg, Mg_3Sb_2 particles formed before α-Mg and Mg_4Zn_7 phase during solidification. Therefore, the distribution of Mg_3Sb_2 phases at the liquid–solid interface would restrict the growth of grains during solidification and thus refine the microstructure. The relatively high-magnification SEM images of as-cast Mg–Zn–Sb alloys and EDS results are shown in Fig. 8 and Table 2. The eutectic structure (α-Mg + Mg_4Zn_7) growing on Mg_3Sb_2 particles could be found effortlessly in alloys. Figure 9 shows the EPMA elemental mapping images for as-cast Mg–6Zn–0.8Sb alloys. The aggregation areas of Sb are almost consistent with those of Zn. The above results suggest that Mg_3Sb_2 particles could act as the substrates for the growth of Mg_4Zn_7 phases and thus significantly refine the microstructure. This coating phenomenon was also found in the researches of Alizadeh et al. [15, 16] and Zou et al. [19]. At first, the refinement effect increased with increasing Sb content and the best refinement effect can be achieved by adding 0.8 wt% Sb. Then, considerable rod-like Mg_3Sb_2 phases started to form and led to coarse microstructure with further increase of Sb content.

4.2 Thermal and Electrical Conductivity

In the Mg–xZn–ySb (x = 0, 2, 4, 6; y = 0, 0.2, 0.5, 0.8, 1.2) alloys, second phases were sparsely distributed without

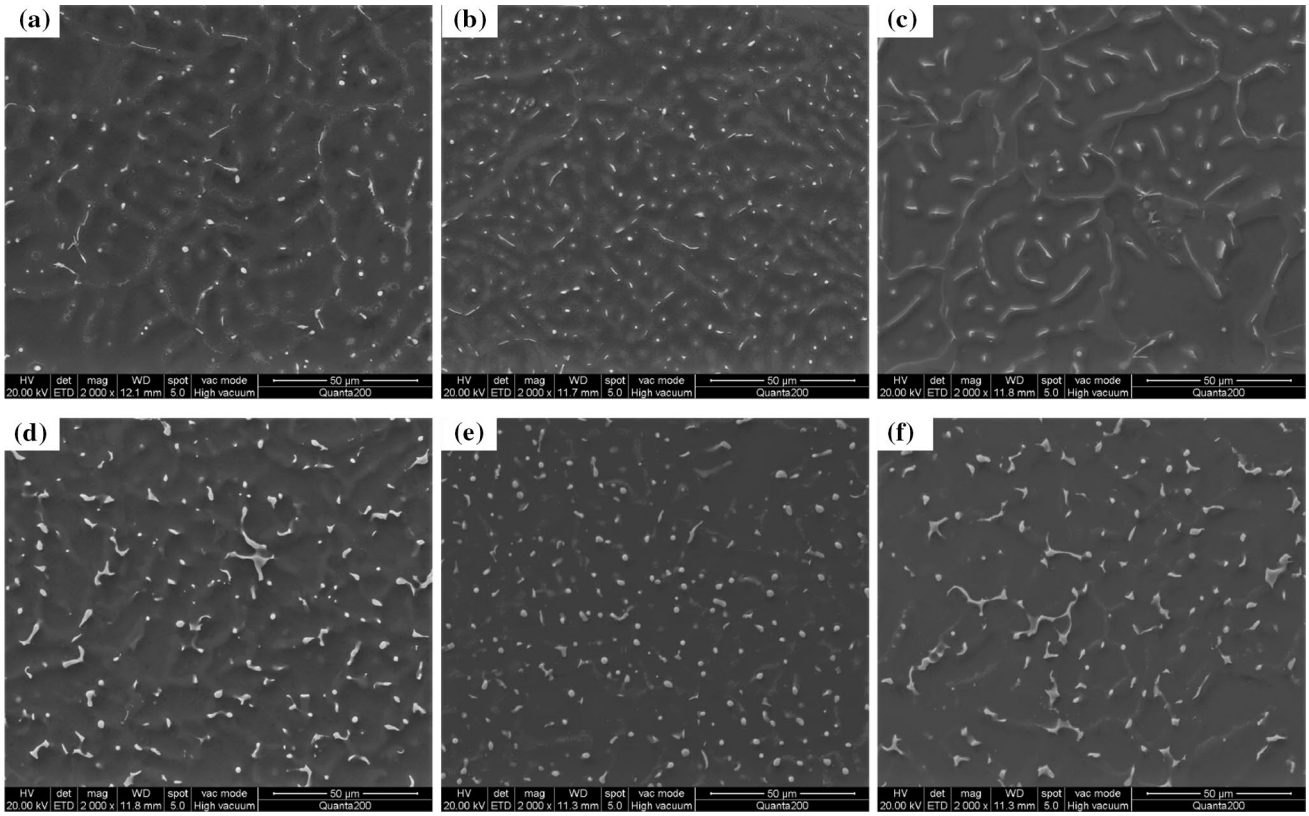

Fig. 5 SEM images of as-cast **a** Mg–2Zn–0.5Sb, **b** Mg–2Zn–0.8Sb, **c** Mg–2Zn–1.2Sb, **d** Mg–6Zn–0.5Sb, **e** Mg–6Zn–0.8Sb, **f** Mg–6Zn–1.2Sb alloys

Table 2 The EDS elemental compositions of points A and B in Fig. 8a

Elements (at%)	A	B
O	9.41	18.63
Mg	80.80	67.86
Zn	9.29	3.44
Sb	0.50	10.07

forming a continuous network of eutectic structure. Therefore, the microstructure can be regarded as common dispersive phases ($Mg_4Zn_7 + Mg_3Sb_2$) of various shapes distributed in another continuous phase (Mg matrix), which applies to the modified Maxwell model proposed by Hamilton [20]. The effective thermal conductivity of the mixture $\lambda_{Maxwell}$ is thereby given by:

$$\lambda_{Maxwell} = \lambda_C \left[\frac{\lambda_P + (n-1)\lambda_C - (n-1)V_P(\lambda_C - \lambda_P)}{\lambda_P + (n-1)\lambda_C + V_P(\lambda_C - \lambda_P)} \right] \quad (2)$$

where λ_C and λ_P are the thermal conductivity of the continuous and dispersive phases, respectively, n is the factor that depends on the shape of dispersed particles and the ratio of the conductivity of the two phases, and V_p is the volume fraction of the dispersed phase.

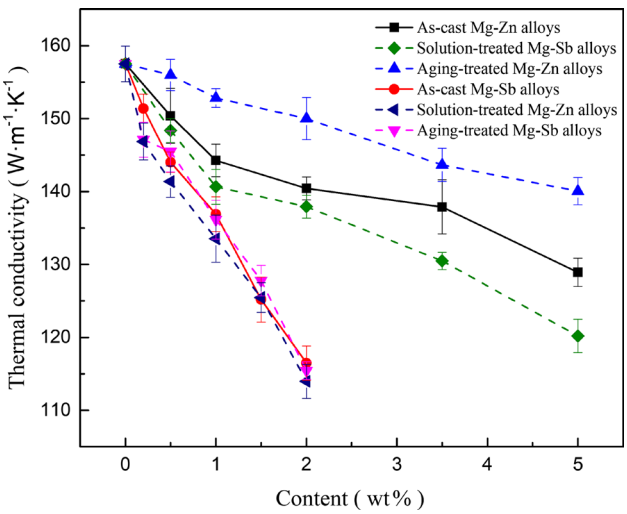

Fig. 6 The thermal conductivity of as-cast Mg–Zn alloys, as-cast Mg–Sb alloys, aging-treated Mg–Zn alloys, aging-treated Mg–Sb alloys, solution-treated Mg–Zn alloys and solution-treated Mg–Sb alloys

Recently, Su et al. [10] proposed that the reduction in thermal conductivity per at% addition of RE alloying elements in solid solution is about 123.0 W/(m·K), and

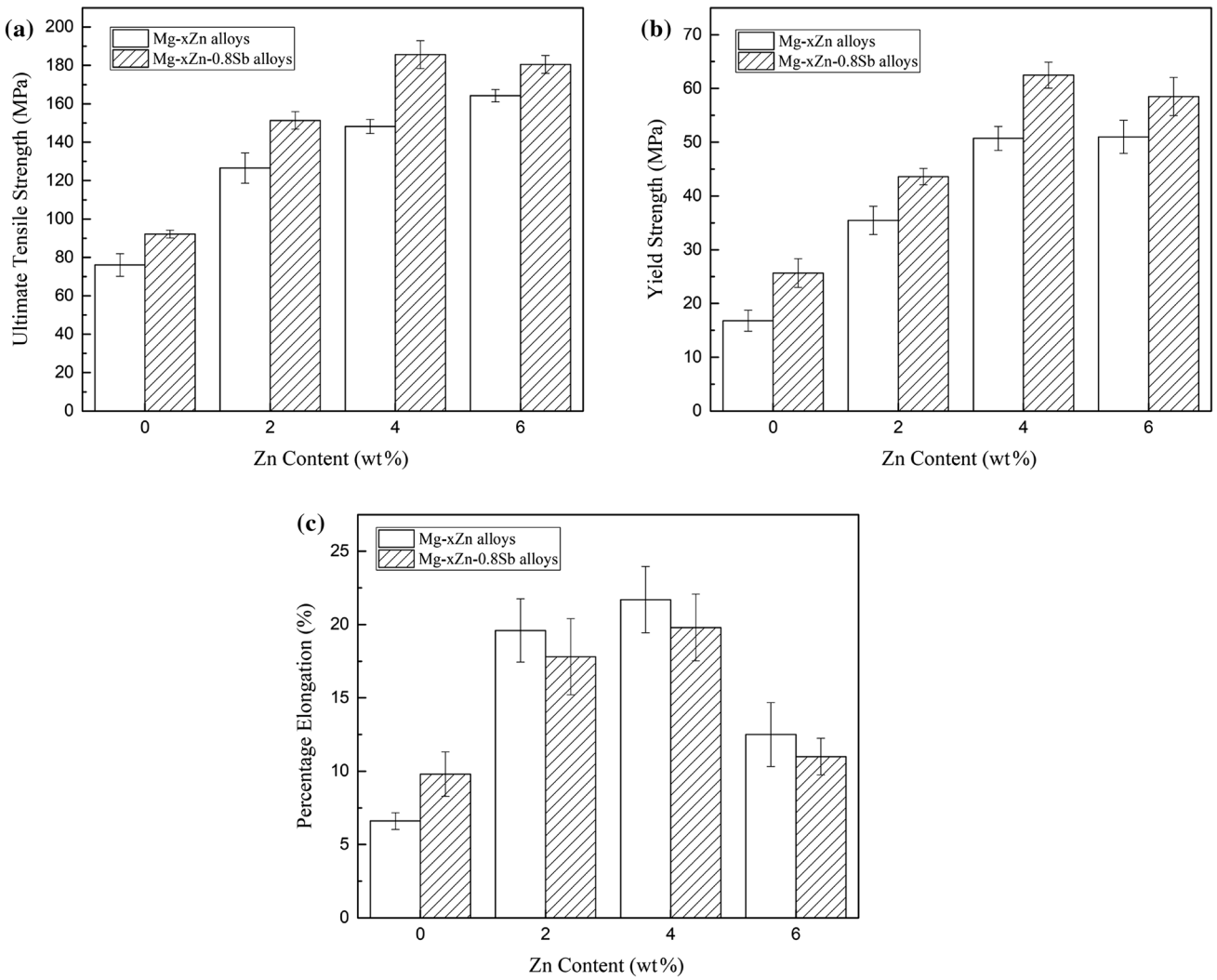

Fig. 7 Tensile properties of as-cast Mg–xZn and Mg–xZn–0.8Sb alloys **a** ultimate tensile strength, **b** yield strength, **c** percentage elongation

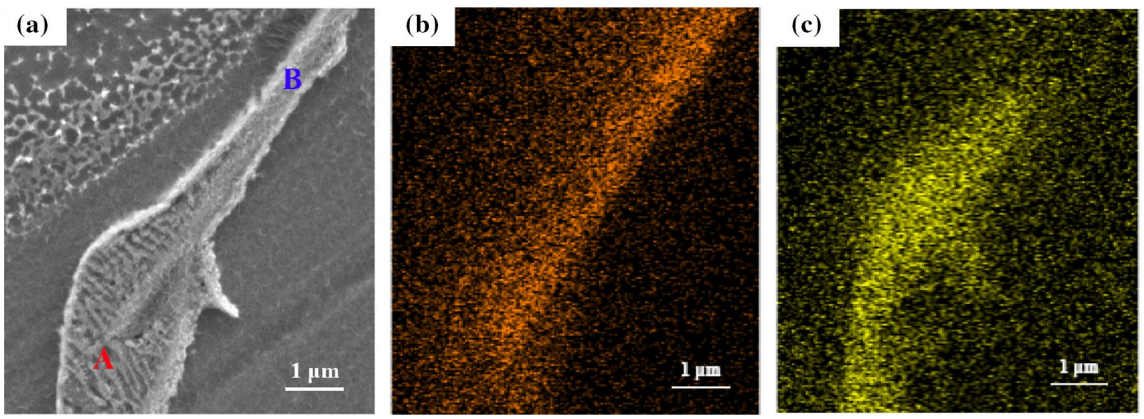

Fig. 8 SEM images and EDS elemental mapping of **a** as-cast Mg–6Zn–0.8Sb alloys, **b** Sb in as-cast Mg–6Zn–0.8Sb alloys, **c** Zn in as-cast Mg–6Zn–0.8Sb alloys

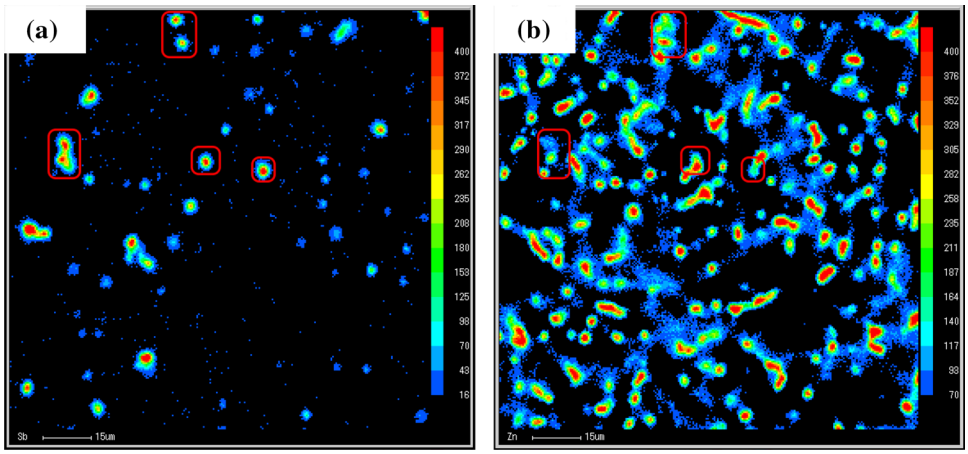

Fig. 9 EPMA elemental mapping of **a** Sb in as-cast Mg–6Zn–0.8Sb alloys, **b** Zn in as-cast Mg–6Zn–0.8Sb alloys. The framed areas are examples of overlapping areas of Sb and Zn

therefore the relationship between the thermal conductivity of the Mg-RE (Ce, Nd, Sm, Y) binary alloys and the RE content in solid solution could be well fitted using a linear function with the slope of − 123. According to the relationship between the content of Zn and thermal conductivity of the solution-treated binary alloys in Fig. 6, the reduction of thermal conductivity per wt% addition of Zn in solid solution is about 17.5 W/(m·K). Similarly, the thermal conductivity of the Mg–Zn–Sb ternary alloys matrix, which deviated from that of pure Mg matrix due to the solute Zn atoms, could be modified by the following formula:

$$\lambda_C = \lambda_{Mg} - 17.5W_{Zn} \quad (3)$$

where λ_{Mg} is the measured thermal conductivity of commercial pure Mg, with a value of 157.51 W/(m·K), W_{Zn} is the solute Zn content in the Mg matrix, obtained by averaging more than 10 EDS results randomly pointed in the middle of Mg matrix. The effect of solute Sb on the thermal conductivity of Mg matrix was ignored because of its negligible solid solubility in Mg matrix.

In the previous research [21], the thermal conductivity of Mg_2Sn, Mg_2Si, and Mg_2Ge second phases were 6.04 W/(m·K), 7.79 W/(m·K), and 6.46 W/(m·K), respectively. Su et al. [10, 22] proposed that the thermal conductivity of second phases were similar so that the thermal conductivity of different second phases could be regarded as an average value in the calculation. Therefore, λ_P, the thermal conductivity of the dispersive phases (α-Mg + Mg_4Zn_7, Mg_3Sb_2 and a mixture of the above two) can be estimated to be the average value 6.8 W/(m·K).

The thermal conductivity of Mg–xZn–ySb (x = 0, 2, 4, 6; y = 0, 0.2, 0.5, 0.8, 1.2) alloys are plotted in Fig. 10 as functions of Sb content. Plots of Eq. (2) were fitted to the experimental results using the least-squares method. The dotted lines are the results calculated by the modified Maxwell model. The best-fit parameter values of n for Mg–ySb, Mg–2Zn–ySb, Mg–4Zn–ySb and Mg–6Zn–ySb were 1.08, 1.09, 1.67 and 1.86, respectively. As shown in Fig. 10, the measured results are in agreement with the calculated ones and the thermal conductivity decreased with the increase of Zn and Sb content.

Generally, the thermal conductivity (λ) of a metal alloy is linked with the electrical conductivity (σ) by the well-known Wiedemann–Franz law $\lambda/\sigma = LT$, where L is the Lorenz number and T is the absolute temperature. L was regarded to be the Summerfeld Lorenz constant $L_0(=2.44\times10^{-8}\ V^2\ K^{-2})$ in all metal alloys without considering its material and temperature dependence. Therefore, Smith and Palmer [23] suggested a more accurate relationship between the thermal conductivity (λ) of a metal alloy and the electrical conductivity as follows:

$$\lambda = AL_0T\sigma + B \quad (4)$$

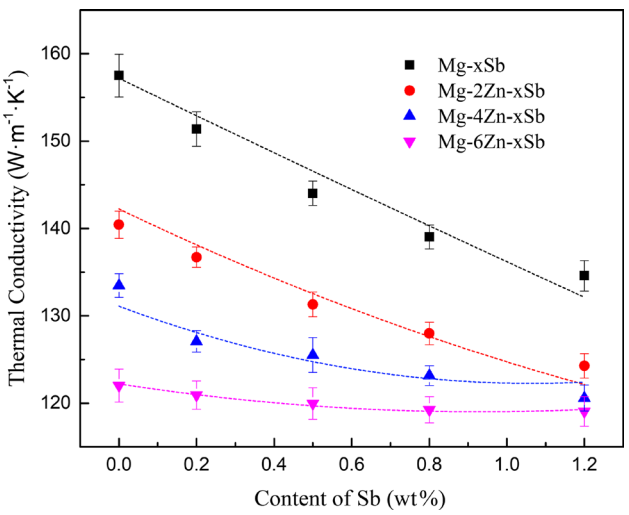

Fig. 10 Thermal conductivity of as-cast Mg–Zn–Sb alloys. The dashed lines represent the values fitted using the modified Maxwell model for Mg–Zn–Sb alloys

where parameter A illustrates the difference of the Lorenz number between alloys and B is the constant lattice thermal conductivity.

According to the previous research [24], the Smith–Palmer equation could well correlate the thermal conductivity with the corresponding electrical conductivity in Mg–Zn Alloys. Figure 11 demonstrates the Smith and Palmer (S–P) plot for Mg–Zn–Sb alloys at 298 K. Apparently, the thermal conductivity of Mg–Zn–Sb ternary alloys could be well described by the S–P equation with A = 0.905 and B = 6.5 W/(m·K). The corresponding Lorenz number L_c (= AL_0) is equal to 2.208×10^{-8} V^2 K^{-2}, and the lattice thermal conductivity B is equal to 6.5 W/(m·K).

4.3 The Interactive Effect of Zn/Sb

It is worth noting that the negative effect of Sb addition on the thermal conductivity of alloys is getting smaller with increasing Zn content. According to thermal conduction mechanism [25], the thermal conduction of metals is dominated by free electrons. The mean free path of electrons determined by the scattering during their movement significantly affects the thermal conductivity of metals. The solute atoms in the matrix cause lattice distortion, decrease the mean free path of electrons and thus reduce the thermal conductivity of alloys. In addition, second phases also act as scattering resources and reduce the thermal conductivity of alloys. The different effects of different solute elements on thermal conductivity have been extensively studied, while the different effects of different second phases were usually masked due to the relatively slighter reduction caused by second phases. Hence, the different effects of Mg_4Zn_7 and Mg_3Sb_2 phases on the thermal conductivity of Mg–Zn–Sb ternary alloys were worth considering in the present study.

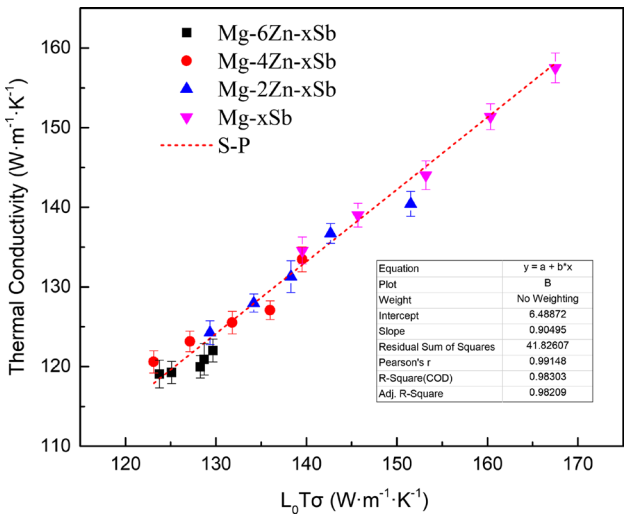

Fig. 11 Smith and Palmer plot for Mg–Zn–Sb alloys

To avoid the influence caused by solute atoms and investigate the different degree in the reduction of thermal conductivity caused by Mg_4Zn_7 and Mg_3Sb_2 phases, the samples of Mg–Zn and Mg–Sb binary alloys were aging treated for precipitating solute atoms. As shown in Fig. 6, the thermal conductivity of aging Mg–Zn alloys was significantly higher than that of as-cast alloys with the same composition due to the precipitation of solute atoms, while the thermal conductivity of aging Mg–Sb alloys was almost the same as that of as-cast alloys due to the negligible solid solubility of Sb in Mg matrix. Besides, it is obvious that the thermal conductivity of aging Mg–Sb alloys is lower than that of Mg–Zn alloys with the same alloying content. For aging binary alloys, Mg matrix is pure without distortion and only Mg_4Zn_7 or Mg_3Sb_2 phases have an effect on the thermal conductivity of alloys. Thus, the relationship between the thermal conductivity of aging alloys and alloying content (wt%) can be reflected in that between the thermal conductivity of aging alloys and the volume fraction of second phases (ρ (Mg_4Zn_7) = 4.9 g/cm^3, ρ (Mg_3Sb_2) = 3.94 g/cm^3) in Fig. 12. Similarly, the thermal conductivity of aging Mg–Sb alloys is still lower than that of Mg–Zn alloys with the same volume fraction of second phases. The lower thermal conductivity of aging Mg–Sb alloys indicates that Mg_3Sb_2 phases are stronger scattering resources than Mg_4Zn_7 phases. Furthermore, according to the above explanation, Mg_3Sb_2 phases could be the substrates for the precipitated Mg_4Zn_7 phases, suggesting that some Mg_3Sb_2 phases, which are stronger scattering resources, could be coated by Mg_4Zn_7 phases, which are relatively weaker scattering resources. When the Zn content in Mg–Zn–Sb alloys is more than 4 wt% and lots of Mg_4Zn_7 phases are precipitated, the Mg_4Zn_7/α-Mg interface would be the dominate scattering interface instead of Mg_3Sb_2/α-Mg interface. With increasing Zn content, the reduction of thermal conductivity caused by Sb addition became smaller due to the coating of Mg_4Zn_7 phases on Mg_3Sb_2 phases. Therefore, the addition of Sb in Mg–Zn alloys has different effects on the thermal conductivity of the alloys with different Zn content.

4.4 Tensile Properties

The beneficial effect of Sb addition on the tensile properties of Mg–Zn alloys can be mainly attributed to the second phase and fine grain strengthening. According to the above explanation, the fine and uniform microstructure was obtained due to the formation of thermally stable Mg_3Sb_2 second phases after adding Sb into Mg–Zn alloys. In addition, the growth of Mg_4Zn_7 phases on Mg_3Sb_2 particles can break the coarse Mg_4Zn_7 phases in the alloys with a high content of Zn and promote the dispersed distribution of Mg_4Zn_7 phases. Therefore, Sb addition can improve the ultimate tensile properties and yield strength of Mg–Zn alloys.

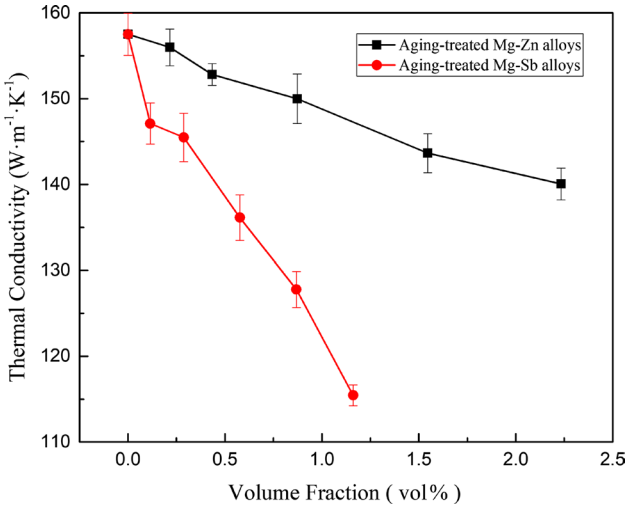

Fig. 12 The thermal conductivity of aging-treated Mg–Zn alloys and aging-treated Mg–Sb alloys with different volume fraction of second phases

Moreover, the refined microstructure could partly offset the negative effect of Mg_3Sb_2 phases on the ductility of alloys. Thus, the percentage elongation of alloys decreased little after adding Sb.

5 Conclusions

In this study, the effects of Sb addition and Zn content on the microstructure, tensile properties and thermal conductivity of Mg–Zn–Sb ternary alloys were evaluated. The main conclusions are as follows:

1. Mg–Zn–Sb ternary alloys consist of α-Mg, Mg_4Zn_7 and Mg_3Sb_2 phases. Mg_3Sb_2 phases could serve as the substrates for the growth of eutectic structure (α-Mg + Mg_4Zn_7), resulting in the refinement of the microstructure. The best refinement effect can be achieved by adding 0.8 wt%Sb. Then the refinement effect decreased with further increase of Sb content due to the formation of considerable rod-like Mg_3Sb_2 phase.
2. The thermal conductivity of Mg–Zn–Sb alloys decreased with increasing Sb content. Both the modified Maxwell model and the Smith–Palmer equation can describe the thermal conductivity of Mg–Zn–Sb alloys quite well.
3. There existed an interactive effect of Zn/Sb on the thermal conductivity of the Mg–Zn–Sb alloys. The effect of Sb addition on the reduction of thermal conductivity was getting smaller with increasing Zn content. The negative effect of Mg_3Sb_2 phases on the thermal conductivity of the alloys could be weakened by the formation of weak-scattering Mg_4Zn_7 coated on Mg_3Sb_2 phases.
4. The addition of 0.8 wt%Sb could effectively increase the strength but decrease the ductility of Mg–Zn alloys. Considering the thermal conductivity of alloys, Mg–4Zn–0.8Sb alloy possess the best comprehensive properties with thermal conductivity of over than 120 W/(m·K) and UTS of 185.6 MPa.

References

1. V.V. Ramalingam, P. Ramasamy, M.D. Kovukkal, G. Myilsamy, Metals Mater. Int. **51**, 1–22 (2019)
2. P.G. Klemens, R.K. Williams, Int. Mater. Rev. **31**, 197–215 (1986)
3. G. Yuan, G. You, S. Bai, W. Guo, J. Alloys Compd. **766**, 410–416 (2018)
4. B.H. Choi, B.S. You, W.W. Park, Y.B. Huang, I.M. Park, Metals Mater. Int. **9**, 395–398 (2003)
5. T. Ying, M. Zheng, Z. Li, X. Qiao, S. Xu, J. Alloys Compd. **621**, 250–255 (2015)
6. J.W. Yuan, K. Zhang, X.G. Li, T. Li, Y.J. Li, M.L. Ma, G.L. Shi, M. Li, L. Lai, Mater. Sci. Forum **319–324**, 198–205 (2000)
7. H. Pan, F. Pan, R. Yang, J. Peng, C. Zhao, J. She, Z. Gao, A. Tang, J. Mater. Sci. **49**, 3107–3124 (2014)
8. T. Ying, H. Chi, M. Zheng, Z. Li, C. Uher, Acta Mater. **80**, 288–295 (2014)
9. A. Eivani, H. Ahmed, J. Zhou, J. Duszczyk, Metall. Mater. Trans. A **40**, 2435–2446 (2009)
10. C. Su, D. Li, A.A. Luo, T. Ying, X. Zeng, J. Alloys Compd. **747**, 431–437 (2018)
11. G. Nayyeri, R. Mahmudi, Mater. Sci. Eng., A **527**, 669–678 (2010)
12. Y. Guangyin, S. Yangshan, D. Wenjiang, Scripta Mater. **43**, 1009–1013 (2000)
13. S.G. Tian, K.Y. Sohn, H.G. Cho, K.H. Kim, Mater. Sci. Forum **488**, 749–752 (2005)
14. M. Ünal, Int. J. Cast. Metals Res. **27**, 80–86 (2014)
15. R. Alizadeh, R. Mahmudi, Mater. Sci. Eng., A **527**, 3975–3983 (2010)
16. R. Alizadeh, R. Mahmudi, Mater. Sci. Eng., A **527**, 5312–5317 (2010)
17. W. Parker, R. Jenkins, C. Butler, G. Abbott, J. Appl. Phys. **32**, 1679–1684 (1961)
18. H.I. Mohamed, M.E. Moussa, M.A. Waly, G.S. Al-Ganainy, A.B. Ahmed, M.S. Talaat, J. Surf. Eng. Mater. Adv. Technol. **7**, 69 (2017)
19. C.M. Zou, Y.M. Zhang, W. Wei, H.W. Wang, Z. Wei, B.G. Fu, T. Nonferr, Metal. Soc. **21**, s222–s228 (2011)
20. R.L. Hamilton, O. Crosser, Ind. Eng. Chem. Fund. **1**, 187–191 (1962)
21. Y.S. Touloukian, *Thermophysical Properties of Matter. Thermal Conductivity: Metallic Elements and Alloys*, vol. 1 (Plenum Press, New York, 1970)
22. C. Su, D. Li, A.A. Luo, R. Shi, X. Zeng, Metall. Mater. Trans. A **50**, 1970–1984 (2019)
23. C.S. Smith, E. Palmer, Trans. AIME **221**, 225–241 (1935)
24. H. Pan, F. Pan, X. Wang, J. Peng, J. Gou, J. She, A. Tang, Int. J. Thermophs. **34**, 1336–1346 (2013)
25. N. Burger, A. Laachachi, M. Ferriol, M. Lutz, V. Toniazzo, D. Ruch, Prog. Polym. Sci. **61**, 1–28 (2016)

Publisher's Note Springer Nature remains neutral with regard to jurisdictional claims in published maps and institutional affiliations.